Journal of Solid State Chemistry 187 (2012) 75–82

Contents lists available at SciVerse ScienceDirect

Journal of Solid State Chemistry

journal homepage: www.elsevier.com/locate/jssc

Structural chemistry and spin-glass behaviour of $Nd_{18}Li_8Fe_4TiO_{39}$

Nirawat Thammajak [a], Peter D. Battle [a,*], Fernande Grandjean [b], Gary J. Long [c], Silvia Ramos [d]

[a] Inorganic Chemistry Laboratory, Department of Chemistry, University of Oxford, South Parks Road, Oxford OX1 3QR, UK
[b] Faculty of Sciences, University of Liège, B-4000 Sart-Tilman, Belgium
[c] Department of Chemistry, Missouri University of Science and Technology, University of Missouri, Rolla, MO 65409-0010, USA
[d] Diamond Light Source, Harwell Science and Innovation Campus, Didcot, Oxfordshire OX11 0DE, UK

ARTICLE INFO

Article history:
Received 21 September 2011
Received in revised form
15 December 2011
Accepted 23 December 2011
Available online 3 January 2012

Keywords:
Mixed-metal oxide
XANES
Spin glass

ABSTRACT

$Nd_{18}Li_8Fe_4TiO_{39}$ has been synthesised and characterised by neutron powder diffraction, X-ray absorption spectroscopy, Mössbauer spectroscopy and magnetometry. The cubic structure ($Pm\bar{3}n$, a=11.97227(8) Å) is based on intersecting ⟨1 1 1⟩ chains comprised of alternating octahedral and trigonal-prismatic coordination sites. These chains lie within hexagonal-prismatic cavities formed by a Nd–O framework. The larger of the two crystallographically distinct octahedral sites, 8*e*, is occupied by iron, titanium and lithium in a ratio of 76:20:4; the smaller, 2*a*, is occupied by iron and titanium in a ratio of 79:21. The trigonal-prismatic site, 16*i*, is occupied by lithium and iron in a ratio of 98:2. The cations on the 2*a* sites are assigned as $Ti^{4+}$and low-spin Fe^{4+}, and those on the 16*i* sites as Li^+ and Fe^{3+}. The 8*e* sites are thought to be occupied by Li^+, Fe^{3+} and Ti^{3+}. $Nd_{18}Li_8Fe_4TiO_{39}$ undergoes a transition to a spin-glass state at 4.25(5) K.

© 2012 Elsevier Inc. All rights reserved.

1. Introduction

The crystal structure drawn in Fig. 1 was first described in detail in an account [1] of the synthesis and characterisation of $Ln_{18}Li_8Rh_5O_{39}$ (Ln=La, Pr). The cubic unit cell (space group $Pm\bar{3}n$) was found to contain ⟨1 1 1⟩ chains of alternating RhO_6 octahedra and LiO_6 prisms, with adjacent polyhedra being linked by face-sharing. The chains intersect at the origin and the body centre of the unit cell, and each chain segment occupies a hexagonal-prismatic cavity within the *Ln*–O framework. The octahedra are not all equivalent; those centred on the 2*a* sites at (0, 0, 0) and $(\frac{1}{2},\frac{1}{2},\frac{1}{2})$ are significantly smaller than those centred on the 8*e* sites at $(\frac{1}{4},\frac{1}{4},\frac{1}{4})$ and equivalent positions. The multiplicity ratio of these two octahedral sites, 1:4, is the same as the ratio of Rh^{4+}:Rh^{3+} cations in $Ln_{18}Li_8Rh_5O_{39}$ and Frampton et al. [1] therefore proposed that these mixed-valence oxides exhibit an ordered arrangement of Rh^{4+} and Rh^{3+}. Subsequent research has shown that this structure type can accommodate a wide range of chemical compositions [2–6]; rhodium may be substituted by various combinations of titanium, manganese, iron, cobalt or ruthenium, with Ln=lanthanum, praseodymium or neodymium.

Much of this research has been undertaken in an attempt to prepare new magnetic materials. The existence of two distinct crystallographic sites sufficiently different in size to induce the ordering of two cation species is reminiscent of the spinel structure, wherein the ordering over two sites of two cations having different magnetic moments results in ferrimagnetism. We therefore hoped that, for example, the 8*e* and 2*a* sites of $LnLi_8Fe_4MnO_{39}$ might accommodate an ordered arrangement of Fe^{3+} and Mn^{4+}, and that ferrimagnetism would consequently be observed below some Curie temperature. However, none of the compositions prepared to date has shown the requisite cation ordering. In the case of $Nd_{18}Li_8Fe_5O_{39}$, the 2*a* site is occupied only by Fe^{4+}, but a small fraction of the Fe^{3+} cations, instead of simply filling the 8*e* sites, undergoes partial site exchange with Li^+ and consequently occupies trigonal-prismatic 16*i* sites [2]. In other cases, for example $Nd_{18}Li_8Fe_4MnO_{39}$, the same lithium/iron exchange occurs and, in addition, the 2*a* site is not exclusively occupied by one element, but by a disordered array of iron and manganese, leaving the 8*e* site occupied by a mixture of lithium, iron and manganese [3]. As a consequence of this structural disorder, and also the existence of competing superexchange interactions involving the *Ln* sublattice, many of the compounds studied, including $Nd_{18}Li_8Fe_5O_{39}$ and $Nd_{18}Li_8Fe_4MnO_{39}$, behave as spin glasses with $T_g \sim 8$ K.

Although the studies referred to above have not produced new magnetic materials, we have made a number of interesting observations, most notably that this structure is able to stabilise cations in unusual oxidation states and spin states. In all but one of the compounds studied to date [4], the Fe^{4+} cations on the 2*a* site adopt a low-spin configuration and the magnetic susceptibility of

* Corresponding author. Fax: +44 1865 272690.
E-mail address: peter.battle@chem.ox.ac.uk (P.D. Battle).

0022-4596/$ - see front matter © 2012 Elsevier Inc. All rights reserved.
doi:10.1016/j.jssc.2011.12.029

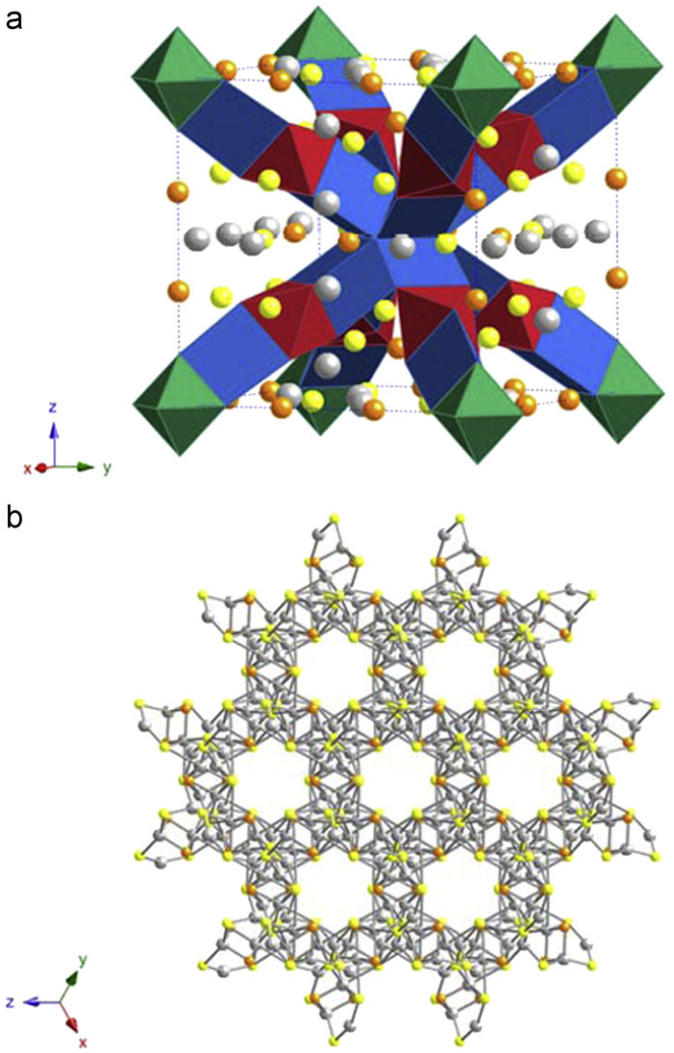

Fig. 1. (a) Polyhedral representation of the cubic (space group $Pm\bar{3}n$) structure of $La_{18}Li_8Rh_5O_{39}$; LiO_6 trigonal prisms are blue (16*i* site), RhO_6 octahedra are green (2*a*) and red (8*e*), grey circles represent oxygen (O2 and O3), yellow circles La1 and orange circles La2. (b) The La–O2–O3 framework viewed along ⟨1 1 1⟩; the polyhedral chains run through the channels. (For interpretation of the references to colour in this figure legend, the reader is referred to the web version of this article.)

$Nd_{18}Li_8Fe_{5-x}Mn_xO_{39}$ [3] is best interpreted by assuming that the Mn^{3+} cations on the 8*e* sites are in a low-spin state. The oxidation state Fe^{4+} is relatively rare in oxide chemistry but when it does occur the cation usually adopts a high-spin state; Mn^{3+} is not rare, but it is also usually found in a high-spin state in oxides. However, both of these cations have been shown to adopt a low-spin state under high pressure [7,8]. Similarly, Ru^{3+}, which we believe to be present in a low concentration in $Pr_{18}Li_8Fe_4RuO_{39}$ [4] and $La_{18}Li_8Rh_4RuO_{39}$ [6], has been stabilized under high-pressure conditions [9]. We have therefore proposed that the *Ln*–O framework illustrated in Fig. 1(b) exerts a significant chemical pressure on the polyhedral chains that occupy the hexagonal cavities within the framework and we have begun to explore the possibility of introducing into the octahedral sites metals that might not be expected to be compatible with the structure under normal conditions. Our initial study of titanium-containing materials focussed on cation-deficient compositions [10] and those containing no other magnetic 3*d* cations [6], but we are now able to report the magnetic properties of $Nd_{18}Li_8Fe_4TiO_{39}$.

2. Experimental

A polycrystalline sample of $Nd_{18}Li_8Fe_4TiO_{39}$ was synthesised using a solid-state technique. Stoichiometric quantities of predried neodymium(III) oxide (99.99%, Alfa Aesar), iron(III) oxide (99.99%, Alfa Aesar), and titanium(IV) oxide (99.995%, Alfa Aesar) were ground together with a 50% excess of volatile lithium carbonate (AnalaR) prior to firing in pellet form at 800 °C in air for 12 h. A further 50% excess lithium carbonate was ground into the reaction mixture before it was fired again in air for 1 h, as a pellet, at 1000 °C.

The progress of the reaction was monitored by X-ray powder diffraction. High-resolution X-ray powder diffraction data for use in quantitative analysis were collected from the final product over the angular range $5 \leq 2\theta/^\circ \leq 125$. The X-ray scattering from the material is dominated by the heavy metals and consequently it was not possible to perform a full structural analysis using these data. Limited Rietveld [11] refinements were carried out using the GSAS [12] suite of programs in order to determine the unit-cell parameter. Backgrounds were fitted using a Chebyshev polynomial of the first kind and the peak shape was modelled using a pseudo-Voigt function.

The diffractometer D2b at the Institut Laue Langevin, Grenoble, France was used to collect neutron powder diffraction data using a wavelength of 1.59460(2) Å. The unit-cell parameter derived from X-ray diffraction data was used to calibrate the neutron wavelength. Data were collected over the angular range $5 \leq 2\theta/^\circ \leq 160$ with a step size $\Delta 2\theta = 0.05^\circ$ at room temperature. The sample (~0.5 g) was contained in a vanadium can of diameter 5 mm. Rietveld refinement of the structure was carried out using the FULLPROF [13] program. The background level was determined by linear interpolation between a set of background points with refinable heights. Peak shapes were modelled using a pseudo-Voigt function together with a correction for peak asymmetry.

Magnetic measurements were carried out using a Quantum Design MPMS 5000 SQUID magnetometer. The sample magnetisation was measured as a function of temperature on warming from 2 to 300 K after cooling both in zero field (ZFC) and in the measuring field of 100 Oe (FC). The isothermal magnetisation was measured as a function of field ($-50 \leq H/\mathrm{kOe} \leq 50$) at 2, 10 and 50 K after cooling to the measuring temperature in 50 kOe. AC susceptibility data were recorded at 4 frequencies ($1 \leq \omega/\mathrm{Hz} \leq 1000$) in a direct field of 1.96(1) Oe, measured using a gadolinium(III) oxide standard, and an oscillating field of amplitude 3.5 Oe over an appropriate temperature range with $\Delta T = 0.1$ K.

X-ray absorption experiments were conducted on beamline B18 at the Diamond Light Source [14]. XANES spectra were collected at the iron *K*-edge of $Nd_{18}Li_8Fe_4TiO_{39}$ and the isostructural compounds $Nd_{18}Li_8Fe_5O_{39}$ and $La_{18}Li_8Fe_5O_{39}$. Data were also collected on Fe_2O_3 (99.99%, Alfa Aesar) as a standard. All samples were diluted with an appropriate amount of cellulose and pressed into a pellet which was held in a pulse tube cryostat at 1.5 K. The measurements were performed in fluorescence mode using a high-rate, nine-element germanium solid-state detector system. A titanium metal foil was used to calibrate the energy scale of the spectrometer at the Ti *K*-edge, 4.966 keV. Energy steps as small as 0.35 eV were employed near the absorption edges with a counting time of 1 s per step. The program Athena was subsequently used for background correction and normalisation [15].

The iron-57 Mössbauer spectra of $Nd_{18}Li_8Fe_4TiO_{39}$ have been measured between 25 and 295 K with a constant-acceleration spectrometer which utilised a rhodium-matrix cobalt-57 source and was calibrated at 295 K with α-iron powder. The Mössbauer spectral absorber contained 20 mg cm^{-2} of the sample powder mixed with boron nitride. The ideal thickness of the Mössbauer absorber is limited to this value because of the strong non-resonant

scattering of the γ-rays by the 18 neodymium ions per formula unit. This is, at least in part, responsible for the rather low signal to noise ratio observed. For the 8*e* site the relative statistical errors associated with the isomer shifts, quadrupole splittings, and line widths are ± 0.005, ± 0.01, and ± 0.01 mm/s, respectively; these errors are approximately twice as large for the 2*a* and 16*i* sites. The absolute errors of these parameters are approximately twice the statistical errors.

3. Results

X-ray powder diffraction indicated that a single-phase product had formed. The data could be accounted for using a structural model based on $Ln_{18}Li_8Rh_5O_{39}$ and the unit-cell parameter refined to a value of 11.97227(8) Å. The neutron diffraction data, which revealed the presence of unreacted lithium carbonate, were analysed using the same structural model. We note that the neutron scattering lengths of iron and titanium are very different (9.51 and −3.35 fm, respectively) and the distribution of these two elements over multiple crystallographic sites can therefore be determined reliably by this method. The results of our analysis, in which all the cation sites were constrained to be fully occupied, are summarised in Table 1. The 2*a* site is occupied predominantly by iron, but with some titanium present. The 8*e* site is occupied by the remainder of the titanium, iron and a small amount of lithium, and the trigonal-prismatic 16*i* site is largely occupied by lithium with a small amount of iron present. No problems were encountered in refining the structure of the neodymium–oxygen framework, which involves Nd1, Nd2, O2 and O3. The displacement parameter of Nd2 is negative but within one standard deviation of zero; this parameter refined to a comparable value of 0.00(5) Å^2 in the titanium-free composition $Nd_{18}Li_8Fe_5O_{39}$ [2].

Table 1
Structural parameters of $Nd_{18}Li_8Fe_4TiO_{39}$ at room temperature.

a (Å)		11.97227(8)
R_{wp}		0.0263
χ^2		1.60
Nd1	*y*	0.3079(4)
24*k* (0 *y* *z*)	*z*	0.3053(4)
	B_{iso} (Å^2)	0.50(5)
Nd2	*x*	0.3489(3)
12*f* (*x* 0 0)	B_{iso} (Å^2)	−0.04(7)
Fe1(Ti)	B_{iso} (Å^2)	0.6(3)
2*a* (0 0 0)	Fe occupancy	0.79(2)
	Ti occupancy	0.21(2)
Fe2(Ti/Li)	B_{iso} (Å^2)	1.2(1)
8*e* ($\frac{1}{4}$ $\frac{1}{4}$ $\frac{1}{4}$)	Fe occupancy	0.76(2)
	Ti occupancy	0.197(6)
	Li occupancy	0.04(1)
Li1(Fe)	*x*	0.369(1)
16*i* (*x* *x* *x*)	B_{iso} (Å^2)	1.3(4)
	Li occupancy	0.977(7)
	Fe occupancy	0.023(7)
O1	*x*	0.8646(4)
48*l* (*x* *y* *z*)	*y*	0.8598(4)
	z	0.6931(3)
	B_{iso} (Å^2)	0.85(5)
O2	B_{iso} (Å^2)	0.8(2)
6*d* ($\frac{1}{4}$ $\frac{1}{2}$ 0)		
O3	*x*	0.6304(6)
12*g* (*x* 0 $\frac{1}{2}$)	B_{iso} (Å^2)	0.6(1)
O4	*x*	0.1536(9)
48*l* (*x* *y* *z*)	*y*	0.015(3)
	z	0.022(2)
	B_{iso} (Å^2)	2.0(4)
	Occupancy	1/4

The low values are consistent with the hypothesis that there is a significant chemical pressure within this structure. The oxide ions O1 and O4 form the shared faces of the polyhedra around the 16*i* site and the 8*e* and 2*a* sites, respectively. There is nothing remarkable about O1 but, as observed and discussed [10] in the case of many other members of this structural family, the oxide ion O4 was found to be disordered over a 25%-occupied 48*l* (*x*, *y*, *z*) site; in the idealised structure O4 would fully occupy a 12*f* (*x*, 0, 0) site. The relatively high displacement parameters of the 8*e* and 16*i* sites are consistent with the disordered occupation of these sites by cations with a significant variation in ionic radius. In contrast to the case of the cation-deficient titanium-containing compositions studied previously [10], trial refinements showed the anion sublattice of $Nd_{18}Li_8Fe_4TiO_{39}$ to be fully occupied. The observed and calculated diffraction profiles are shown in Fig. 2 and the refined bond lengths are listed in Table 2.

The temperature dependence of the dc magnetic susceptibility shows no hysteresis between the ZFC and FC data at high temperatures. The data in the temperature range $165 < T/K < 300$

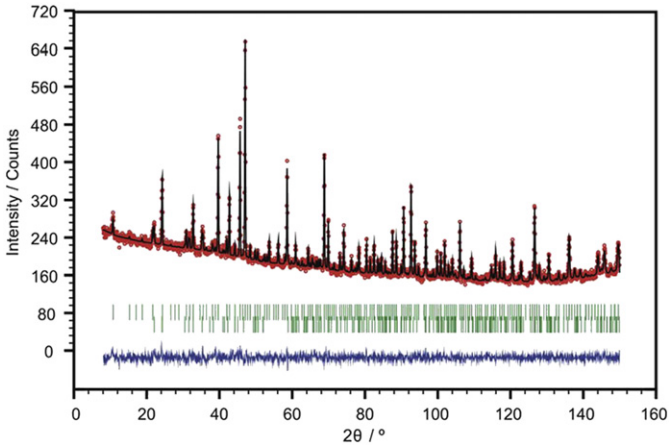

Fig. 2. Observed and calculated room-temperature neutron diffraction profiles of $Nd_{18}Li_8Fe_4TiO_{39}$; a difference curve is also shown. Upper and lower tick marks indicate the positions of reflection positions from Li_2CO_3 and the main phase, respectively.

Table 2
Bond lengths (Å) and bond angles (deg.) in $Nd_{18}Li_8Fe_4TiO_{39}$ at room temperature.

Nd1–O1	2.637(6) × 2
	2.581(7) × 2
	2.497(5) × 2
Nd1–O2	2.432(5)
Nd1–O3	2.425(5)
	3.110(5)
Nd2–O1	2.387(5) × 4
Nd2–O3	2.390(6) × 2
Nd2–O4	2.360(13)
Fe1(Ti)–O4	1.867(13) × 6
Fe2(Ti)–O1	2.019(5) × 6
Li1–O1	2.112(13) × 3
Li1–O4	2.24(2) × 3[a]
Li1–Li1	3.132(17)
Fe1(Ti)–Li1	2.712(12)
Fe2(Ti)–Li1	2.472(12)
Nd1–Nd1 (pore size)	6.285(2)
O1–Fe2(Ti)–O1	89.8(1)
	89.9(1)
	93.6(1)

[a] The average bond length to a disordered oxygen site.

could be fitted to a Curie–Weiss law with $C=52.93(7)\,cm^3\,mol^{-1}$ and $\theta=-12.1(3)\,K$. A maximum is apparent in the ZFC susceptibility at 4.25(5) K (see Fig. 3), and the FC susceptibility is approximately constant below this temperature. Hysteresis is apparent in the field dependence of the magnetisation at 2 K, shown in Fig. 4. At 10 K no hysteresis is apparent but $M(H)$ is clearly not a linear function, whereas at 50 K the linearity expected of a paramagnet is observed. The results of our ac susceptibility measurements (see Fig. 5), show that the temperature of the susceptibility maximum, T_f, is frequency dependent and that the susceptibility has an imaginary component below 6 K. The frequency dependence of the susceptibility maximum can be parameterised [16] as $\Delta T_f/T_f\Delta\log\omega=0.047$. As is shown in Fig. 6 for 1 and 1000 Hz, at all measured frequencies the maximum in the real component of the susceptibility coincides with the minimum in the gradient of the imaginary component.

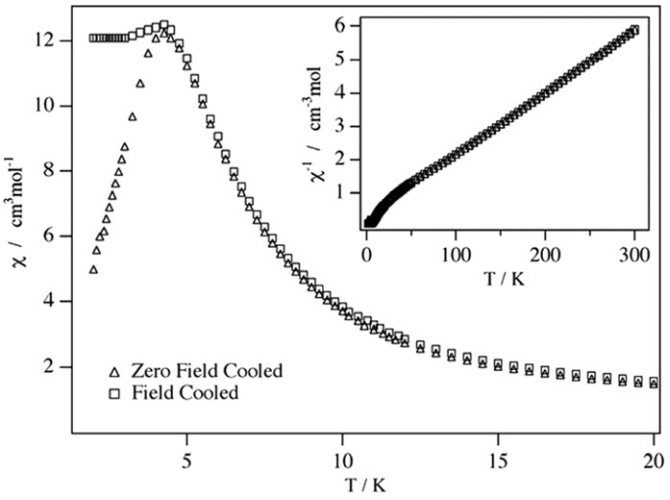

Fig. 3. Temperature dependence of the dc molar magnetic susceptibility of $Nd_{18}Li_8Fe_4TiO_{39}$. The inset shows the temperature dependence of the inverse susceptibility.

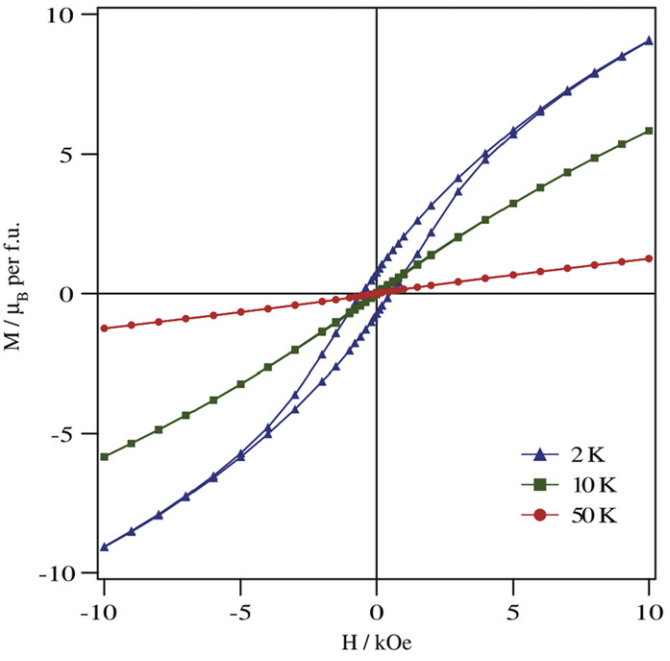

Fig. 4. Field dependence of the magnetisation per formula unit of $Nd_{18}Li_8Fe_4TiO_{39}$ at 2, 10 and 50 K.

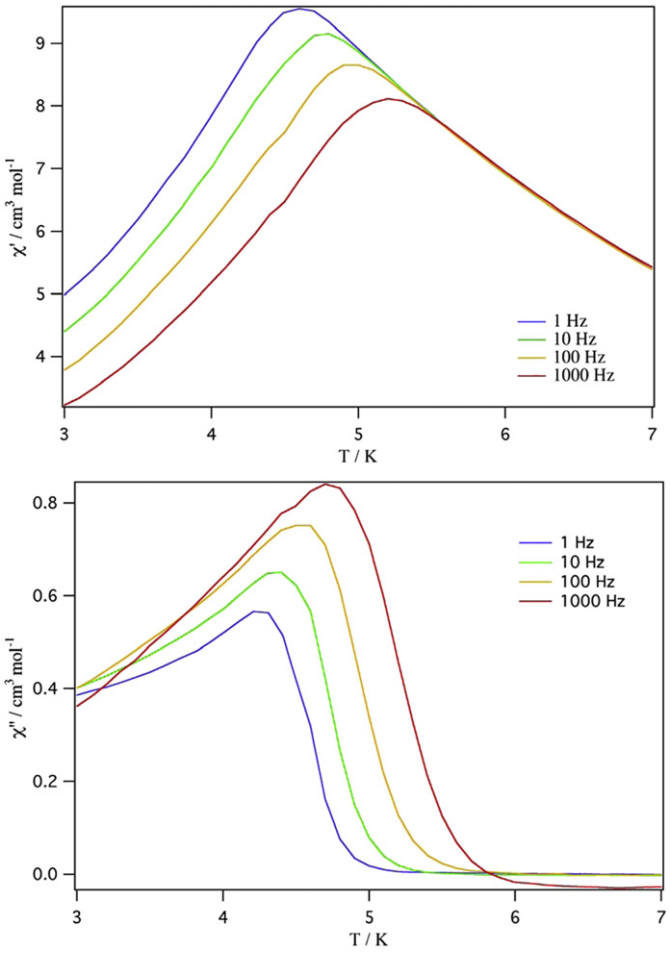

Fig. 5. Temperature and frequency dependence of the real and imaginary components of the ac molar susceptibility of $Nd_{18}Li_8Fe_4TiO_{39}$. (The reader is referred to the web version of this article, where colour is used to distinguish between the different frequencies.)

Fig. 7 shows the measured iron *K*-edge X-ray absorption spectra and the differential of each spectrum with respect to energy. For all of the compounds isostructural with $Ln_{18}Li_8Rh_5O_{39}$ the derivative shows features at 7123.5 eV and 7127 eV that coincide with local maxima in the data derived from Fe_2O_3. However, the maximum at 7129 eV in the derivatives of the spectra of $Ln_{18}Li_8(M,M')_5O_{39}$ is not apparent in the data from Fe_2O_3.

The iron-57 Mössbauer spectra of $Nd_{18}Li_8Fe_4TiO_{39}$ have been measured between 25 and 295 K; selected spectra are shown in Fig. 8 and the remaining spectra are very similar to those shown. The spectra indicate that $Nd_{18}Li_8Fe_4TiO_{39}$ is paramagnetic between 25 and 295 K; there is no indication of the onset of any magnetic ordering at 25 K. The spectra have all been fit with three doublets assigned to the 2*a*, 8*e*, and 16*i* sites, see Table 3; the relative areas of these doublets have been constrained to values that correspond to the iron occupancy of these crystallographic sites as determined at room temperature by powder neutron diffraction (see Table 1).

The isomer shifts observed for $Nd_{18}Li_8Fe_4TiO_{39}$ are comparable with those observed [2] for the similar $Nd_{18}Li_8Fe_5O_{39}$ compound with the possible exception of the 2*a* site, occupied by low-spin Fe^{4+}, at lower temperatures. The temperature dependence of the isomer shifts of the 8*e* and 16*i* sites, and the weighted average isomer shifts (see Fig. 9), have been fit with the Debye model [17] for the second-order Doppler shift with characteristic Mössbauer temperatures, Θ_M^{δ}, of 660(20), 620(10) and 740(30) K, values that

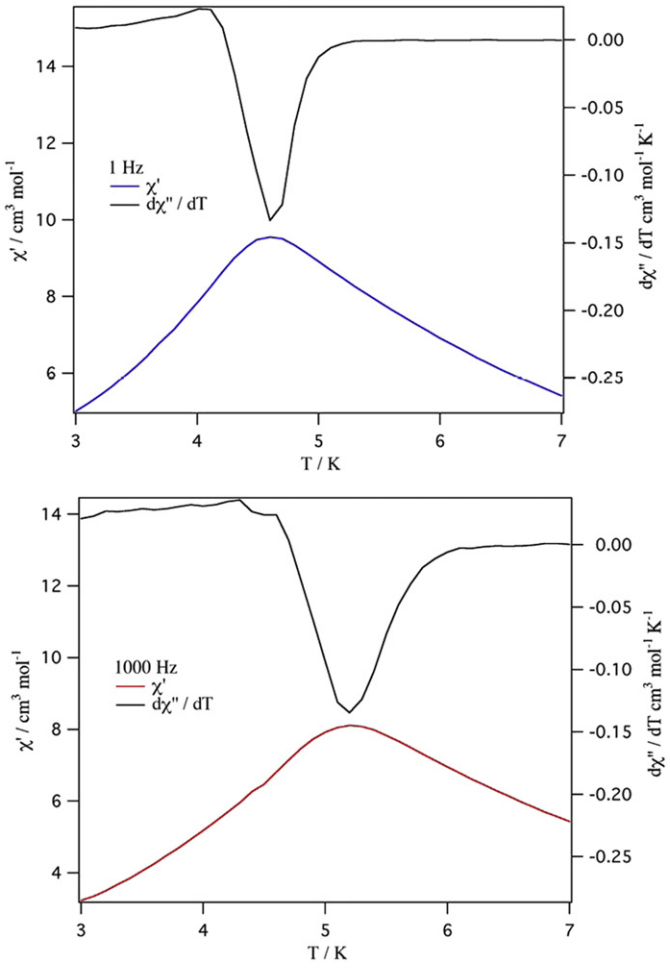

Fig. 6. Temperature dependence of χ' and $d\chi''/dT$ of $Nd_{18}Li_8Fe_4TiO_{39}$ at measuring frequencies of 1 and 1000 Hz. (The reader is referred to the web version of this article, where colour is used to distinguish between the susceptibility and the differential with respect to temperature.)

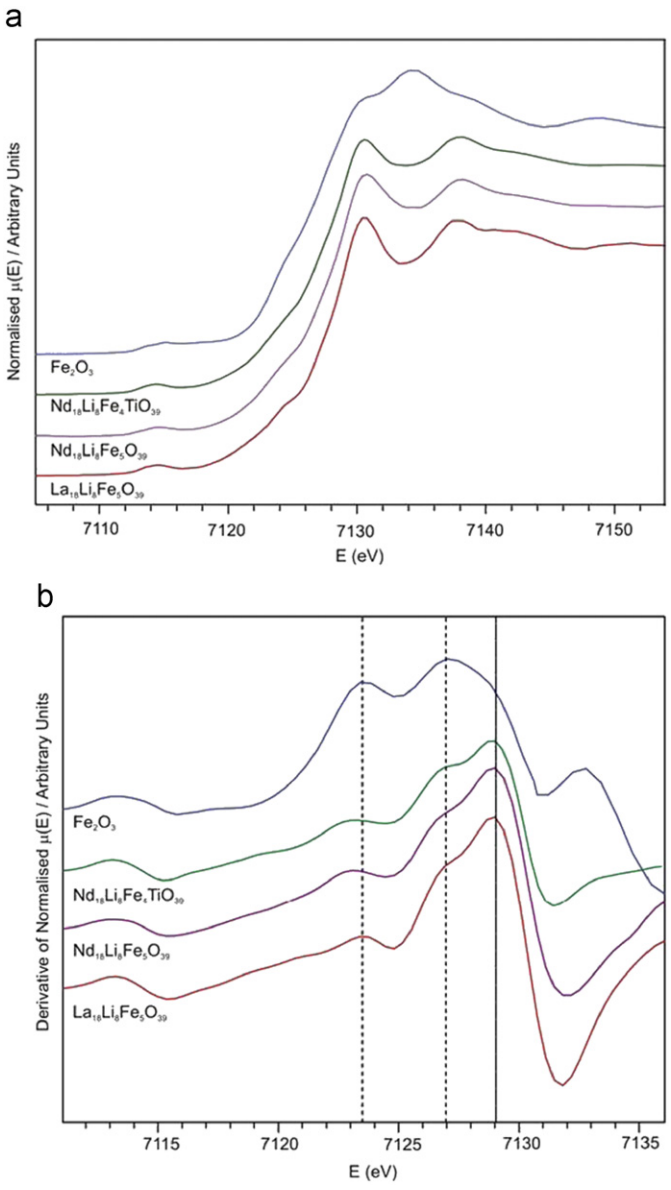

Fig. 7. (a) X-ray absorption spectra of $Nd_{18}Li_8Fe_4TiO_{39}$ and related compounds at 1.5 K. (b) Energy dependence of the differential of X-ray absorption by $Nd_{18}Li_8Fe_4TiO_{39}$ and related compounds with respect to energy at 1.5 K.

are typical of oxidic six-coordinate high-spin Fe^{3+} complexes [18–21]. In contrast, it is not possible to obtain a similar fit between 25 and 295 K for the 2*a* site because the 25 and 60 K isomer shifts for this site are lower than would be expected; a fit from 140 to 295 K yields a Θ_M^δ temperature of 840(130) K for the 2*a* site.

The temperature dependence of the quadrupole splittings of the 2*a*, 8*e*, 16*i* sites and their weighted average, for $Nd_{18}Li_8Fe_4TiO_{39}$ is shown in Fig. 10. There is little temperature dependence of the quadrupole splitting for the 8*e* and 16*i* sites, again consistent with their accommodating high-spin Fe^{3+} cations. The green line in Fig. 10 corresponds to a fit of the quadrupole splitting of the 2*a* site with the Ingalls model [22] for the splitting, Δ, by a low symmetry component of the crystal field, of the three nominally degenerate t_{2g} orbitals in an Fe^{4+} complex; the best fit yields $\Delta = 410(15)\,cm^{-1}$. However, it should be noted that at 25 and 60 K the quadrupole splitting of the 2*a* site is slightly lower than might be expected, indicating that the above Δ value may not be applicable.

The temperature dependence of the logarithm of the Mössbauer spectral absorption area observed for $Nd_{18}Li_8Fe_4TiO_{39}$ is shown in Fig. 11. The fit in this figure yields a Mössbauer temperature, Θ_M^A, of 410(15) K, a value that is substantially smaller than the Θ_M^δ values obtained from the temperature dependence of the isomer shifts. It is well known [17,18] that the two temperatures, Θ_M^δ and Θ_M^A, obtained from the two temperature dependencies, are usually different because they depend on $\langle v^2 \rangle$ and $\langle x^2 \rangle$, respectively, where $\langle v^2 \rangle$ is the mean-square vibrational velocity of the iron-57 nuclide and $\langle x^2 \rangle$ is the mean-square displacement of the iron-57 nuclide; unfortunately, there is no model-independent relationship [18] between these mean-square values. However, the values of these temperatures reported [17] for other iron complexes indicate that Θ_M^δ, which is more sensitive to the high-frequency phonons, is often two to four times larger than Θ_M^A, as is the case for $Nd_{18}Li_8Fe_4TiO_{39}$.

Finally, we note that our sample of $Nd_{18}Li_8Fe_4TiO_{39}$ no longer appeared to be monophasic when studied by X-ray diffraction after storage in air for 3 years. A somewhat older sample of $Nd_{18}Li_8Fe_5O_{39}$ was still monophasic.

4. Discussion

The results described above show that titanium can be substituted for 20% of the iron in $Nd_{18}Li_8Fe_5O_{39}$ to form $Nd_{18}Li_8Fe_4TiO_{39}$. The X-ray absorption spectra and their derivatives (see Fig. 7), emphasise the similarity in the local environment of the iron cations

in these two compounds and show that the same oxidation states of iron are present in all three of the $Ln_{18}Li_8(M,M')_5O_{39}$ compounds studied, thus leading to the conclusion that $Nd_{18}Li_8Fe_4TiO_{39}$ contains both Fe^{3+} and Fe^{4+}. The features at 7123.5 eV and 7127 eV in $d\mu(E)/dE$ are also found in the Fe_2O_3 standard and are hence attributed to the presence of Fe^{3+} ions. The maximum in $d\mu(E)/dE$ at 7129 eV observed in the case of the $Ln_{18}Li_8(M,M')_5O_{39}$ compounds but not in that of Fe_2O_3 can probably be attributed to the presence of Fe^{4+}. We note that the maximum in the differential of the spectrum of $SrFeO_3$ [23], a perovskite containing only Fe^{4+}, occurs at 7127 eV at 25 K, thus making the assignment of the feature at this energy in Fig. 7(b) somewhat ambiguous. Standards for Fe^{4+} are not common and XANES spectra for such a reference sample were not measured specifically for this work. The difference between the position of the maximum assigned to Fe^{4+} for the compounds presented here and the perovskite can be explained in terms of the different temperatures at which the data were collected, the presence of high-spin Fe^{4+} cations in the perovskite and smaller, low-spin Fe^{4+} cations in $Ln_{18}Li_8(M,M')_5O_{39}$ and the presence of corner-sharing and face-sharing octahedra in $SrFeO_3$ and $Ln_{18}Li_8(M,M')_5O_{39}$, respectively; Fe_2O_3 contains Fe^{3+} in both face- and edge-sharing octahedra.

The Mössbauer spectra shown in Fig. 8 are also consistent with the presence of both high-spin Fe^{3+} and low-spin Fe^{4+} in $Nd_{18}Li_8Fe_4TiO_{39}$. Furthermore, the quantity of Fe^{4+} observed in the Mössbauer spectra is consistent with the fraction of the 2*a* sites found by neutron diffraction to be occupied by iron. The presence of Fe^{4+} requires $Nd_{18}Li_8Fe_4TiO_{39}$ to contain both Ti^{4+} and Ti^{3+} cations. Assuming that the smaller cations occupy the smaller 2*a* site, we propose that the 2*a* site is occupied by Fe^{4+} and Ti^{4+} and the 8*e* site predominantly by Fe^{3+} and Ti^{3+}, albeit with a small amount of iron/lithium cation exchange between the 8*e* site and the trigonal-prismatic 16*i* site.

The structural data are consistent with the conclusions drawn from the spectroscopic data. The average bond lengths determined by neutron diffraction in both the Nd–O framework and the polyhedral chains in $Nd_{18}Li_8Fe_4TiO_{39}$ (see Table 2), are not significantly different from those reported previously [2] for $Nd_{18}Li_8Fe_5O_{39}$, suggesting that the cation-ordering scheme adopted in the former allows the replacement of 20% of the iron by titanium with no structural perturbation, despite the differing sizes of the cations involved. The ionic radii relevant to this discussion increase [24] in the sequence $Fe^{4+} < Ti^{4+} < Fe^{3+} < Ti^{3+}$. Arguments based on size grounds alone would predict that Ti^{4+} cations are too large [25] to occupy the 2*a* site in $Nd_{18}Li_8Fe_4TiO_{39}$ without creating considerable structural strain and that this site should be occupied exclusively by Fe^{4+}, as it is

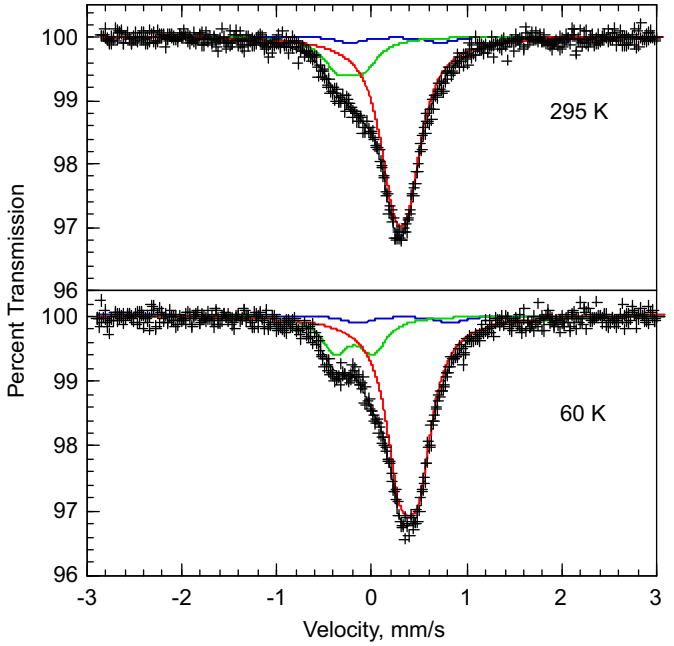

Fig. 8. The iron-57 Mössbauer spectra of $Nd_{18}Li_8Fe_4TiO_{39}$ measured at the indicated temperatures. The green, red, and blue lines correspond to the components assigned to the 2*a*, 8*e*, and 16*i* sites, respectively. (For interpretation of the references to colour in this figure legend, the reader is referred to the web version of this article.)

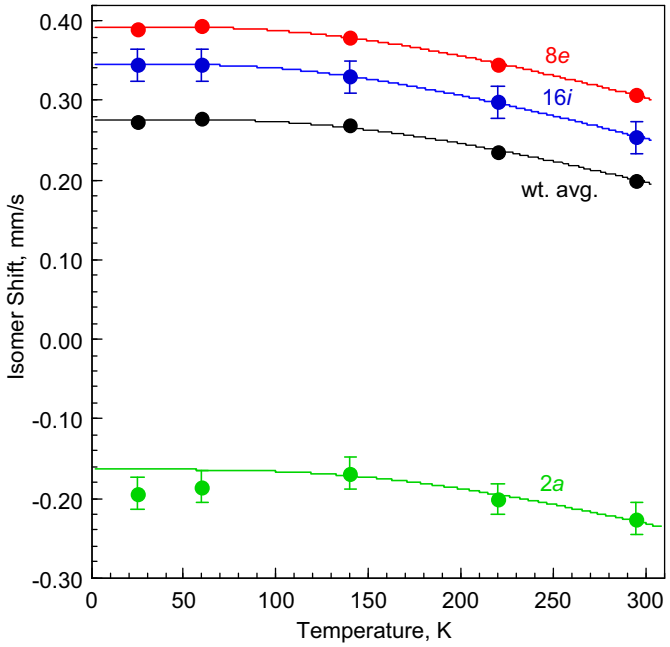

Fig. 9. The temperature dependence of the Mössbauer spectral isomer shifts for the 2*a*, 8*e*, and 16*i* sites, and their weighted average, in $Nd_{18}Li_8Fe_4TiO_{39}$. The solid lines correspond to fits with the Debye model of a solid where the 2*a* site fit includes only the 140, 220, and 295 K isomer shifts. If not shown the errors are at most the size of the data points.

Table 3
Mössbauer spectral parameters for $Nd_{18}Li_8Fe_4TiO_{39}$.

T (K)	2*a* site		8*e* site		16*i* site		Γ (mm/s)	Area, (%ε) × (mm/s)
	δ (mm/s)[a]	ΔE_Q (mm/s)	δ (mm/s)[a]	ΔE_Q (mm/s)	δ (mm/s)[a]	ΔE_Q (mm/s)		
295	−0.226	0.26	0.307	0.15	0.254	0.96	0.38	2.62
220	−0.201	0.36	0.345	0.18	0.296	0.97	0.39	2.79
140	−0169	0.41	0.379	0.19	0.330	0.97	0.37	2.89
60	−0.186	0.40	0.394	0.20	0.345	0.98	0.35	3.08
25	−0.194	0.40	0.390	0.20	0.345	0.98	0.36	3.11

[a] The isomer shifts are given relative to 295 K α-iron powder.

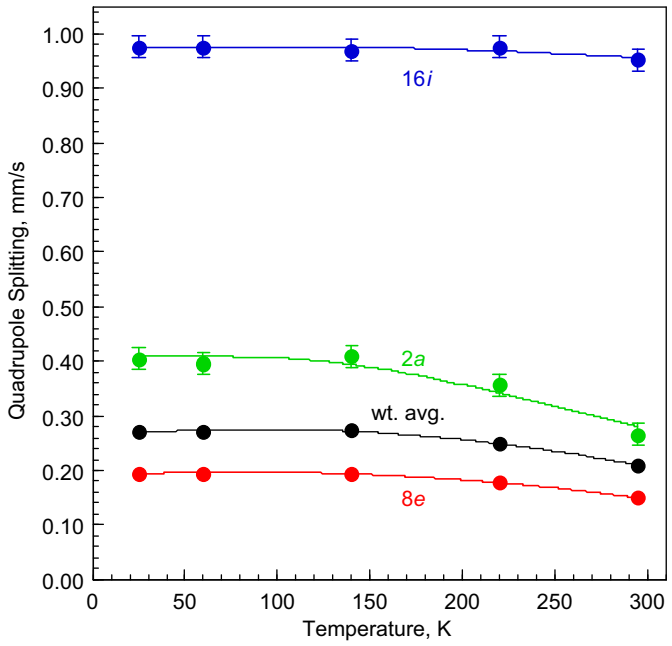

Fig. 10. The temperature dependence of the Mössbauer spectral quadrupole splittings for the 2*a*, 8*e* and 16*i* sites, and their weighted average, in $Nd_{18}Li_8Fe_4TiO_{39}$. The 2*a* site quadrupole splittings have been fit with the Ingalls model; the remaining lines are a guide to the eye. If not shown the errors are at most the size of the data points. (For interpretation of the references to colour in this figure, the reader is referred to the web version of this article.)

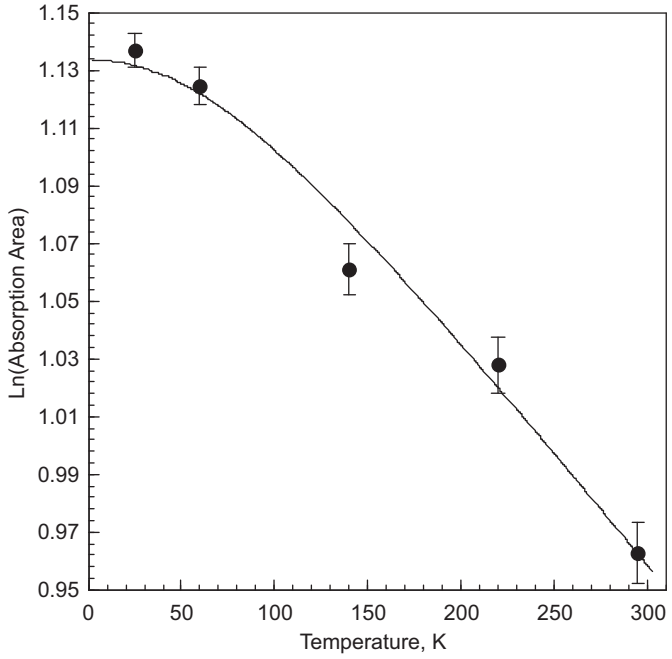

Fig. 11. The temperature dependence of the logarithm of the Mössbauer spectral absorption area of $Nd_{18}Li_8Fe_4TiO_{39}$. The solid line is a fit with the Debye model of a solid.

in $Nd_{18}Li_8Fe_5O_{39}$. In this case all the titanium would have to be trivalent and occupy 8*e* sites. However, the redox chemistry of the elements involved must also be taken into account, and titanium is more readily oxidised to the tetravalent state than is iron. Our data suggest that the relative ease of oxidation of titanium compared to iron prevents the complete removal of titanium from the 2*a* site and the observed structure represents a compromise between two competing effects, ionic size and redox chemistry. This is consistent with the observation that the Ti:Fe ratio of 21:79 on the 2*a* site in $Nd_{18}Li_8Fe_4TiO_{39}$ is lower than the Mn^{4+}:Fe^{4+} ratio of 28:72 [3] in $Nd_{18}Li_8Fe_4MnO_{39}$, Mn^{4+} being intermediate in size between Ti^{4+} and Fe^{4+}. The presence of the two competing factors thus results in the presence of four species of cation in the structure, including the unusual Ti^{3+} and Fe^{4+} oxidation states. The size of the coordination octahedron around the 8*e* site is well matched to the size of Ti^{3+} [26] and the need to minimise structural strain around the 2*a* sites is thus likely to be the most important factor in determining the cation distribution in the present case. This explanation is consistent with the structure of $La_{18}Li_8Rh_4TiO_{39}$ [6] in which 64% of the 2*a* sites and 9% of the 8*e* sites are occupied by titanium as Ti^{4+} and Ti^{3+}, respectively. The difference between the cation distributions in the two compounds stems from the increased size of the 2*a* site when *Ln*=La; the metal-to-oxygen bond length in $La_{18}Li_8Rh_4TiO_{39}$, 1.924 Å, allows the accommodation of Ti^{4+} without excessive strain.

The formation of Ti^{3+} in a mixed-metal oxide under the synthetic conditions described above is unusual. An alternative explanation is that the compound is deficient in either iron or lithium, thus allowing all the titanium to exist as Ti^{4+}. Although a small quantity of unreacted Fe_2O_3 in our sample might not have been detected by X-ray diffraction, it is very unlikely to have escaped detection by magnetometry [27]. If the oxidation of the titanium on the 8*e* site was to be accommodated by a lithium deficiency, then the composition would become $Nd_{18}Li_{7.2}Fe_4TiO_{39}$. However, refinement of the occupancy of the 16*i* site provided no support for this model. We therefore tentatively suggest that $Nd_{18}Li_8Fe_4TiO_{39}$ provides another example of the stabilisation of an unusual oxidation state, Ti^{3+}, by this crystal structure. The presence of the reduced cation might be responsible for the long-term instability of this compound in air.

The low-temperature magnetic properties of $Nd_{18}Li_8Fe_4TiO_{39}$ are very similar to those of $Nd_{18}Li_8Fe_5O_{39}$. The hysteresis between the ZFC and FC dc susceptibilities below the susceptibility maximum (see Fig. 3), together with the field-dependence of the magnetisation (see Fig. 4), the frequency dependence of the real part of the ac susceptibility and the presence of an imaginary component (see Fig. 5), leads us to conclude that a transition from a paramagnetic phase to a spin-glass phase occurs on cooling below T_g=4.25 K. The magnitude of $\Delta T_f/T_f \Delta \log \omega$ is consistent with the formation of an insulating spin glass, as is the coincidence of the maximum in $\chi'(T)$ and the minimum in $d\chi''/dT$ (see Fig. 6). The behaviour of the susceptibility suggests that all the magnetic cations, including the lanthanides, are frozen in the glassy state. Similar behaviour has been seen in isostructural compounds of Nd^{3+} and Pr^{3+} [2–4]; T_g=5.75, 4.5 and 5.0 K, for $Nd_{18}Li_8Fe_5O_{39}$, $Nd_{18}Li_8Fe_4CoO_{39}$ and $Pr_{18}Li_8Fe_4MnO_{39}$, respectively. The absence of a spin-glass transition in isostructural compounds having *Ln*=La [5] leads us to conclude that the magnetic interactions between the *Ln*–O framework and the polyhedral chain segments are an important source of the frustration necessary for the formation of a spin glass. The temperature dependence of the magnetic susceptibility of $Nd_{18}Li_8Fe_4TiO_{39}$ at higher temperatures can be fitted to the Curie–Weiss equation. The value of the Weiss constant, θ=−12.1 K, is unremarkable for this structural family and shows that antiferromagnetic interactions are dominant. However, the value of the Curie constant, C=52.93 $cm^3\ mol^{-1}$, is unusually high. If the effective magnetic moment of the Nd^{3+} cations is calculated assuming that they behave as ideal $^4I_{9/2}$ species, then the value of the Curie constant cannot be explained using any plausible combination of oxidation states and spin states for the *d*-block cations. In order to account for the observed value, we

must assume an enhancement of ~12% in the contribution from the *f*-block cations. This has not been observed in any of the compounds studied previously, and we are unable to explain why it should occur in this compound.

5. Conclusions

$Nd_{18}Li_8Fe_4TiO_{39}$ provides a further illustration of the ability of this crystal structure to accommodate a wide variety of cations, often in unusual oxidation states, in this case Ti^{3+} and Fe^{4+}. In this compound, as in many others studied previously, competing magnetic interactions involving both the *d*-block and *f*-block cations lead to the formation of a spin-glass state at low temperature.

Acknowledgments

We are grateful to Dr. E. Suard for providing experimental assistance at the ILL in Grenoble, France. F.G. acknowledges the financial support of the Fonds National de la Recherche Scientifique, grants 9.456595 and 1.5.064.05. N.T. was supported by a Royal Thai Government Scholarship. We acknowledge useful discussions with Dr. S.E. Dutton.

References

[1] P.P.C. Frampton, P.D. Battle, C. Ritter, Inorg. Chem. 44 (2005) 7138.
[2] S.E. Dutton, P.D. Battle, F. Grandjean, G.J. Long, K. Oh-ishi, Inorg. Chem. 47 (2008) 11212.
[3] S.E. Dutton, P.D. Battle, F. Grandjean, G.J. Long, P.A. van Daesdonk, Inorg. Chem. 48 (2009) 1613.
[4] S.E. Dutton, P.D. Battle, F. Grandjean, G.J. Long, M.T. Sougrati, P.A. van Daesdonk, E. Winstone, J. Solid State Chem. 182 (2009) 1638.
[5] P.D. Battle, S.E. Dutton, N. Thammajak, F. Grandjean, M.T. Sougrati, G.J. Long, K. Oh-ishi, S. Nakanishi, Inorg. Chem. 49 (2010) 5912.
[6] P.D. Battle, S.E. Dutton, P.A. van Daesdonk, J. Solid State Chem. 183 (2010) 1620.
[7] F. Aguado, F. Rodriguez, P. Nunez, Phys. Rev. B 76 (2007) 094417.
[8] M. Takano, S. Nasu, T. Abe, K. Yamamoto, S. Endo, Y. Takeda, J.B. Goodenough, Phys. Rev. Lett. 67 (1991) 3267.
[9] R. Greatrex, G. Hu, D.C. Munro, Mater. Res. Bull. 21 (1986) 797.
[10] P.D. Battle, S.E. Dutton, F. Grandjean, G.J. Long, N. Thammajak, S. Wisetsuwannaphum, J. Solid State Chem. 184 (2011) 2580.
[11] H.M. Rietveld, J. Appl. Crystallogr. 2 (1969) 65.
[12] A.C. Larson, R.B. von Dreele, General Structural Analysis System (GSAS), Los Alamos National Laboratories LAUR 86-748, 1990.
[13] J. Rodriguez-Carvajal, Physica B 192 (1993) 55.
[14] A.J. Dent, G. Cibin, S. Ramos, A.D. Smith, S.M. Scott, L. Varandas, M.R. Pearson, N.A. Krumpa, C.P. Jones, P.E. Robbins, J. Phys.: Conf. Ser. 190 (2009) 012039.
[15] B. Ravel, M. Newville, J. Synchrotron Radiat. 12 (2005) 537.
[16] J.A. Mydosh, Spin Glasses: An Experimental Introduction, Taylor & Francis, London, 1993.
[17] G.K. Shenoy, F.E. Wagner, G.M. Kalvius, in: G.K. Shenoy, F.E. Wagner (Eds.), Mössbauer Isomer Shifts, North-Holland, Amsterdam, 1978, p. 49.
[18] T. Owen, F. Grandjean, G.J. Long, K.V. Domasevitch, N. Gerasimchuk, Inorg. Chem. 47 (2008) 8704.
[19] D.L. Reger, J.R. Gardinier, S. Bakbak, W. Gemmill, M.D. Smith, L. Rebbouh, F. Grandjean, A.M. Shahin, G.J. Long, J. Am. Chem. Soc. 127 (2005) 2303.
[20] D.L. Reger, J.R. Gardinier, M.D. Smith, A.M. Shahin, G.J. Long, L. Rebbouh, F. Grandjean, Inorg. Chem. 44 (2005) 1852.
[21] D.L. Reger, J.D. Elgin, M.D. Smith, F. Grandjean, L. Rebbouh, G.J. Long, Polyhedron 25 (2006) 2616.
[22] R. Ingalls, Phys. Rev. A 133 (1964) 787.
[23] M. Okube, Y. Furukawa, A. Yoshiasa, T. Hashimoto, M. Sugahara, A. Nakatsuka, J. Phys.: Conf. Ser. 121 (2008) 092004.
[24] R.D. Shannon, Acta Crystallogr. A 32 (1976) 519.
[25] Y.A. Abramov, V.G. Tsirelson, V.E. Zavodnil, S.A. Ivanov, I.D. Brown, Acta Crystallogr. B 51 (1995) 942.
[26] S.C. Abrahams, Phys. Rev. 130 (1963) 2230.
[27] F.J. Morin, Phys. Rev. 78 (1950) 819.